48th AIAA Aerospace Sciences Meeting Including the New Horizons Forum and Aerospace Exposition
4 - 7 January 2010, Orlando, Florida

AIAA 2010-626

Pulse Discharge Network Development for a Heavy Gas Field Reversed Configuration Plasma Device

Shawn W. Miller* and Joshua L. Rovey†
Missouri University of Science & Technology, Rolla, Missouri 65409
(formerly University of Missouri-Rolla)

A simple LRC circuit model is used to conduct a parametric study of the effects of charging voltage, capacitance, resistance, and inductance on the current waveform of a pulse forming network for field reversed configuration (FRC) plasma production. Using known waveforms from existing networks, estimates of realistic values of resistance and inductance are established for a base network model. Parametric modification of the base model is used to study the effects of each component of the discharge network. Results indicate that increasing charging voltage causes an increase in peak current, but does not effect rise or reversal times. However, increasing capacitance increases peak current and increases rise and reversal times. Further, optimum circuit parameters are determined for the design and construction of an FRC formation test article. Three main design criteria are used and are based on magnetic diffusion time, auto-ionization of background gas, and peak magnetic field strength. Results indicate that a pulse forming network with charging voltage of 25 kV and capacitance of 1 μF provides the widest range of resistance and inductance values such that the waveform meets the design criteria.

Nomenclature

C	=	circuit capacitance
D	=	coil diameter
g	=	gravitational constant
I_{sp}	=	specific impulse
i	=	current
L	=	circuit inductance or characteristic length
L_{coil}	=	coil inductance
$\dot{m}$	=	mass flow rate
P	=	power
p	=	damping coefficient
R	=	circuit resistance
R_{coil}	=	coil resistance
T	=	thrust
T_e	=	plasma electron temperature (eV)
V_C	=	capacitor voltage
V_L	=	inductor voltage
V_R	=	resistor voltage
v_e	=	exit velocity
W	=	coil width
Z	=	ion charge state
ρ	=	resistivity
ω_o	=	undamped resonant frequency

* Graduate Student Researcher, Department of Mechanical and Aerospace Engineering, 160 Toomey Hall, 400 W. 13th St., Rolla, Mo 65409-0050, (573) 341-6768, AIAA Student Member.
† Assistant Professor of Aerospace Engineering, Department of Mechanical and Aerospace Engineering, 292D Toomey Hall, 400 W. 13th St., Rolla, Mo 65409-0050, (573) 341-4613, Senior AIAA Member.

ω_1 = natural frequency
μ_o = permeability of free space
τ = magnetic diffusion time
η = plasma resistivity
Λ = plasma parameter

I. Introduction

PROPULSION systems having high exhaust velocities (v_e > 10 km/s) are desirable for many space missions. To reduce the amount of propellant required for a given mission, a propulsion system should have an exhaust velocity on the same order as or greater than the characteristic velocity increment (ΔV) required for the mission. Recent studies have shown that for orbit transfer missions, a characteristic velocity increment of over six kilometers per second may be necessary.[1-3] Thus, high specific impulse (I_{sp}) propulsion systems are needed.

The exhaust velocity of chemical propulsion systems is determined by the energy released from chemical bonds of the propellant molecules. Cryogenically-fueled chemical rockets are inherently limited to exhaust velocities below 5 km/s.[4] Chemical rockets which use space storable propellants such as hydrazine are limited to exhaust velocities of about 3 km/s.[4] Chemical rockets do not have the exhaust velocity to meet all future propulsion needs. Thus, propulsion systems that produce exhaust velocities considerably higher than those obtained with chemical systems would greatly enhance a variety of space missions.

To achieve high exhaust velocity, a propulsion system must accelerate its propellant gas without relying on energy addition through chemical reactions. Electric propulsion (EP) devices achieve these exhaust velocities by using electrical energy to accelerate particles to high velocities to generate thrust.[5] In spite of the fact that EP systems have high exhaust velocities, they do not have large thrust levels because of the limited spacecraft power available. This is illustrated by Eqn. 1, which is plotted in Figure 1 for different spacecraft power levels. Fixed spacecraft power requires thrust to decrease as specific impulse increases.

$$P = \frac{1}{2}\dot{m}v_e^2 = \frac{1}{2}TI_{sp}g \qquad (1)$$

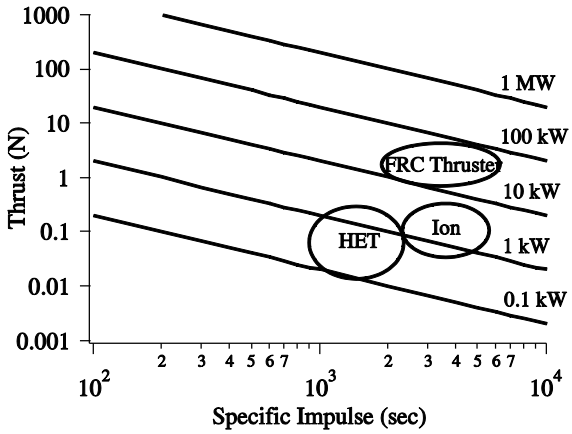

Figure 1. Thrust vs. specific impulse for different spacecraft power levels.

The ability of satellites to rapidly perform space maneuvers, between various orbital inclinations, or between geostationary and low Earth orbits, is a very desirable capability that could be used to create and maintain an operationally responsive space (ORS) environment. The goal of ORS is to provide an affordable capability to promptly, accurately, and decisively position and operate national and military assets in and through space and near-space. To accomplish this objective effectively, a space propulsion system must have high thrust to provide timely placement of space assets, while also possessing high specific impulse to minimize required onboard propellant and spacecraft mass.

An ORS platform based on chemical propulsion can provide the required high thrust. However, chemical rockets are economically questionable due to the short mission lifetime resulting from poor specific impulse. To obtain maximum flexibility and mission lifetime a propulsion system with higher specific impulse is required. As spacecraft power levels increase, an electric propulsion system with both high specific impulse and relatively high thrust becomes an option.

Current state-of-the-art electric propulsion systems (such as Hall thrusters and ion thrusters) have high specific impulse, but significantly lower thrust than chemical systems. The specific impulse and thrust produced by state-of-the-art Hall-effect thrusters (HETs) and ion thrusters for typical spacecraft power levels of 1-10 kW are shown in Figure 1. Simple scaling of these devices to power levels envisioned for future ORS spacecraft (~50 kW) is prohibitive. For example, scaling a single 5 kW HET to 50 kW requires increasing the thruster channel diameter from 17 cm to 46 cm,[6] a factor of 7 increase in the thruster area! While clustering of thrusters has also been explored for higher power spacecraft,[7,8] this also involves prohibitive increases in mass and size. For instance, a cluster of 10, 5 kW thrusters would be required for a 50 kW system.

Instead, a new propulsion system capable of higher thrust density is required to reduce propulsion system mass. For example state-of-the-art ion thrusters and HETs have thrust density on the order of 1-10 N/m^2. A future system must produce at least 50-100 N/m^2. This type of propulsion system must be capable of higher plasma density in order to expel more propellant for a given thruster area, e.g., 10^{14} cm^{-3} as opposed to 10^{11} – 10^{12} cm^{-3} for HET and ion thrusters. One promising approach that is being considered is the field-reversed configuration (FRC) thruster.

In the following sections we describe a parameter study for the initial design of a pulse forming network for an FRC plasma propulsion test article. First, background information about FRC plasma is provided along with the state of the art in FRC propulsion. Then we describe a simple LRC circuit model that is used to represent the pulse forming network. The design criteria used to determine optimum circuit parameters are described. Simulations of the LRC circuit are then used to determine the optimum circuit parameters.

II. Background – Field Reversed Configuration Plasma

The FRC is a specific type of plasma configuration that is more generally known as a compact toroid. Compact toroids (CTs) include both spheromaks, which have toroidal and poloidal magnetic field ($B_z \approx B_\theta$), and FRCs, which have only poloidal field ($B_z >> B_\theta$).[9] Arguably the most important characteristic of CT plasma is the lack of magnetic field lines linking the physical device to the plasma. This property leads to plasma that is formed in a high β configuration, namely the externally applied magnetic pressure balances the interior plasma particle pressure. Ideally, this type of configuration provides efficient containment and energy deposition into the plasma. The following sections provide more information on the physics of FRC formation and current state-of-the-art propulsion results.

A. Device Physics

An FRC thruster has two main processes or stages: 1) FRC formation and 2) FRC acceleration. Thrust is generated through pulsed expulsion of plasma in the form of FRCs. The following description of conventional FRC formation follows the sequence given by Goldenbaum[10] and Bellan[9] and has four main steps: 1) preionization; 2) implosion; 3) reconnection; and 4) equilibrium. The sequence starts with a gas-filled tube and a straight bias magnetic field generated by a slow external coil. Plasma is then created and this effectively pre-ionizes the gas as shown in Figure 2.[9,10]

Next, a fast capacitor bank discharges through the theta coil and creates a reversed magnetic field. The field is reversed on a time-scale that is less than the magnetic diffusion time ("Implosion" in Figure 2). This fast rising implosion field causes radial compression of the initial bias field. The field lines at the ends of the device reconnect and the compressed inner poloidal field necessitates the formation of a toroidal plasma current. At the equilibrium state the FRC is composed of a toroidal plasma current with a poloidal magnetic field and is immersed in the outer poloidal field. It is a magnetically detached compact torus known as an FRC.

The FRC is ideal for space propulsion because external coils are not linked to the plasma and the plasma is on a magnetic island (i.e., completely detached from the spacecraft)

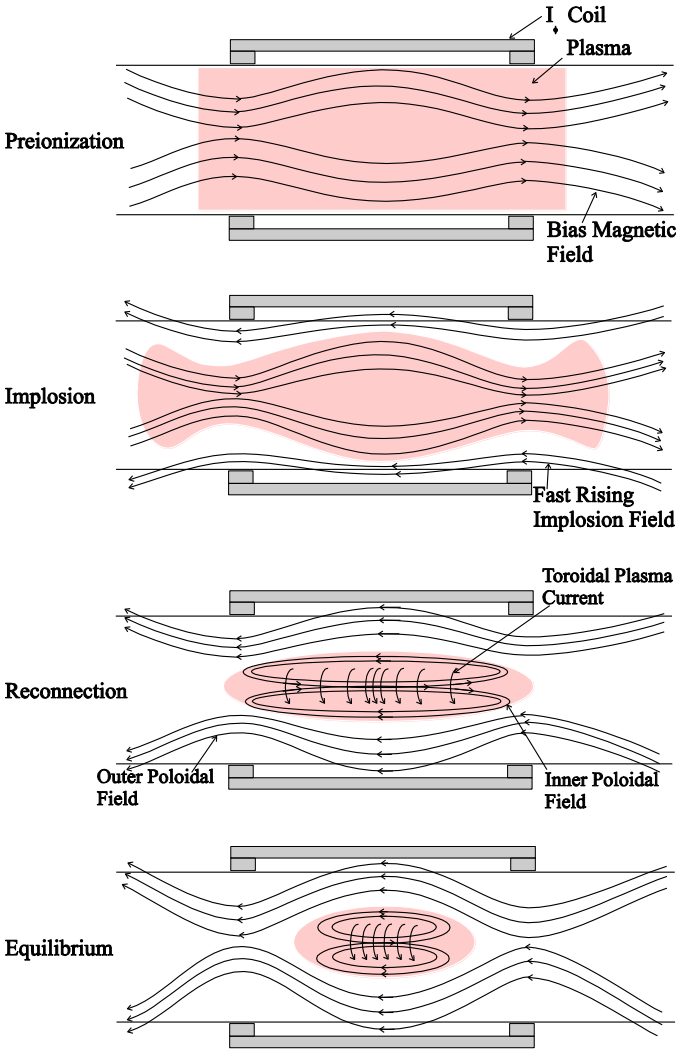

Figure 2. Schematics illustrating FRC formation process.

such that magnetized plasma should not return to the spacecraft. Figure 3 shows a schematic of an FRC. Figure 3 also shows some of the typical characteristics of an FRC, such as separatrix radius and trapped (or excluded) flux.

Acceleration and expulsion of the FRC can be accomplished with a variety of mechanisms. For example, asymmetrically squeezing the magnetic field around the FRC will cause it to accelerate toward the lower field region. In some designs, a series of pulsed magnetic coils is used to accelerate the FRC to an optimum velocity. Further, the formation and acceleration steps can be combined together with the proper design of the pulsed theta coil.

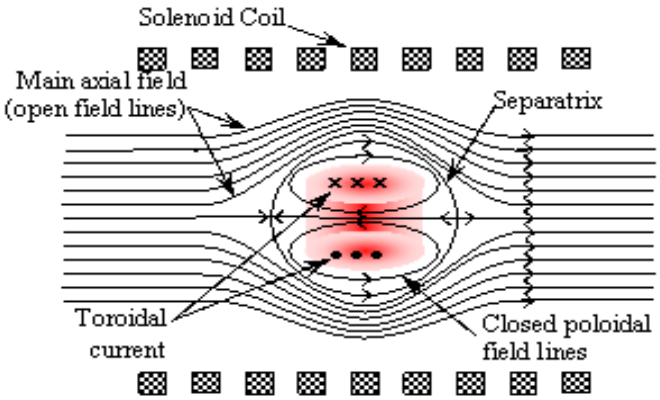

Figure 3. Schematic of a FRC plasma noting the induced toroidal current reversal.

B. State of the Art of FRC Propulsion

Fusion applications of FRCs have been investigated for decades.[11-14] The goal of these investigations was compression and heating of the FRC to achieve *D-T* or *D-He*$_3$ fusion reactions. To achieve fusion temperatures during FRC creation, the plasma was non-adiabatically heated and large densities and temperatures created (e.g., ion temperature T_i = 50-1000 eV, electron temperature T_e = 50-250 eV, and average density n = 10^{15} cm^{-3}).[15] Many of these experiments focused on increasing confinement time, overall dimensions, and plasma density. Further, FRCs have been used to simulate high-temperature plasma instability events in tokomaks. Specifically, in Ref. 16 a conical device with a centerline-peaked pre-ionization plasma was used to create and accelerate FRCs. While it was not designed for propulsion, results indicated expelled plasma velocities of 1.2x10^5 m/s.

FRCs for space propulsion application have been previously investigated at the University of Washington, University of Alabama-Huntsville, and at the Air Force Research Laboratory (AFRL).[17-24] These studies have mainly focused on lower energy FRC formation and translation with higher atomic mass gases. Specific results from these investigations are described next.

Research performed at the University of Washington has investigated the use of FRCs for space propulsion and fusion, both individually and as a combined spacecraft system. Slough, *et.al.*, have investigated the Propagating Magnetic Wave Plasma Accelerator (PMWAC) device for space propulsion[17,18] and also an earth-to-orbit fusion plasmoid device.[19] Both of these have similar operating principles. First, a FRC is created using the method shown in Figure 2. Then the FRC is accelerated using a magnetic wave created by a sequence of pulsed electromagnetic coils. If the device is only providing propulsion, then the accelerated FRC is expelled at high velocity. However, if fusion is desired, then the FRC is compressed to smaller diameter causing the temperature to increase to fusion levels. Power can then be extracted for use creating the next FRC and the process is repeated. Results showed an ejection velocity of at least 1.8x10^5 m/s for each deuterium plasmoid, which yielded a total impulse bit of 0.3 N-s.[17]

The University of Washington in collaboration with MSNW LLC is also developing the Electrodeless Lorentz Force (ELF) thruster. The goal of the ELF device is to demonstrate efficient acceleration of a variety of propellants to high velocities (10-40 km/s) and operation at high power (e.g. >100 kW). The device is designed around a conical geometry with a rotating magnetic field current drive to ionize the gas and drive an azimuthal current to form an FRC.[25]

Investigations at the University of Alabama-Huntsville and NASA Marshall Space Flight Center have centered on the Plasmoid Thruster Experiment (PTX).[23,24,26] PTX produces plasmoids in an analogous fashion to that shown in Figure 2; however, a conical geometry is used instead of cylindrical. This geometry has benefits because the FRC creation and acceleration occur within the same step. Unlike the PMWAC developed by Slough, a traveling magnetic wave is not required to accelerate the FRC. Results have shown electron temperature and density of 7.6 eV, and 5.0x10^{13} cm^{-3} for argon and 23 eV and 1.2x10^{14} cm^{-3} for hydrogen.[23] Exit velocities up to 2.0x10^4 m/s have been measured.

Recently AFRL has become interested in FRCs for space propulsion application. Specifically, the electric propulsion group at Edwards Air Force Base constructed an annular FRC device called XOCOT.[20] The XOCOT project primary goal was to develop FRC-based plasmas at low power with long lifetime for propulsion applications. The program investigated different charging energies, voltages, and timing, as well as multiple propellants and pre-ionization techniques. Results showed multiple plasma formation and implosions are possible with densities and electron temperature on the order of 3.0x10^{13} cm^{-3} and 8 eV, respectively.[22] Current Air Force efforts in

collaboration with Michigan Technological University are focused on understanding and quantifying the acceleration mechanism, plume profile, and plume energy of an FRC thruster.[27]

Each of these FRC devices has demonstrated positive results, affirming the propulsive capabilities of a heavy gas FRC system. The investigation currently underway at Missouri S&T centers on the formation stage of heavy gas FRCs. The objective is to study the efficiency of the formation process with a heavy gas (e.g. argon or xenon), with specific interest in the energy conversion and loss processes. Understanding these processes will aid in determining methods for achieving maximum plasma creation using the least amount of energy. Ideally, energy for ionization would be maximized, thermal energy minimized to the necessary level for ionization, and losses reduced in the FRC formation process. Current work is focused on the design of an FRC test article and development of MHD plasma and radiation modeling capabilities. The following sections describe a parametric study to design a pulse forming network for an FRC test article.

III. Circuit Model

Creation of FRC plasma is typically a pulsed or transient process. The pulse discharge network consists of several components that must be sized in order to achieve desired results. In the following sections we describe a simple LRC circuit model of a pulse forming network for FRC creation. Then estimates of realistic values of resistance and inductance from exiting networks are presented. Finally, the design parameter space investigated is described.

A. LRC Circuits

A simple LRC circuit model is used to assess the effects of pulse forming network voltage and capacitance on important discharge parameters, such as peak current and rise time. Properly selecting the pulse discharge properties is important in order to obtain a waveform that meets the desirable criteria listed below. The following paragraphs describe the LRC circuit model used for the pulse forming network design.

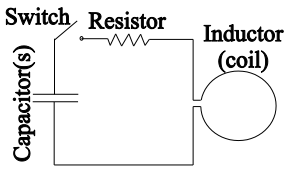

Figure 4. Simple LRC circuit utilized in model.

An LRC circuit consists of an inductor (L), resistor (R), and capacitor (C). For the pulse forming network for the FRC plasma device design, a simple LRC circuit is used and is shown in Figure 4. The switch is initially open and the capacitor is charged to a voltage, $V_c(0)$. At time t = 0, the switch closes and current flows through the circuit. This is a transient pulse and analysis of this problem can be accomplished using transient analysis of a second order circuit.

The capacitor, inductor, and resistor of Figure 4 are in series with each other and Kirchhoff's voltage law can be used to generate Eqn. 2, where V stands for the voltage drop across the component. Using the defining circuit laws for a capacitor and inductor, Eqn. 2 can be rewritten as Eqn. 3. Differentiating Eqn. 3 yields Eqn. 4, which is a 2nd order differential equation. While the presence of plasma in the pulse discharge system suggests that resistance, capacitance, and inductance will all vary with time, we assume constant values for this analysis. The result is that Eqn. 4 is a 2nd order differential equation with constant coefficients and can be solved analytically. There are three possible solutions which lead to either an overdamped, critically damped, or underdamped response based on the criteria of Eqn. 5. Solution of Eqn. 4 yields the current as a function of time through the LRC circuit.

$$V_C(t) + V_R(t) + V_L(t) = 0 \tag{2}$$

$$\frac{1}{C}\int_{-\infty}^{t} i\,dt + iR + L\frac{di}{dt} = 0 \tag{3}$$

$$\frac{d^2 i}{dt^2} + \frac{R}{L}\frac{di}{dt} + \frac{1}{LC}i = 0 \tag{4}$$

$$\left(\frac{R}{L}\right)^2 - \frac{4}{LC} \begin{cases} > 0 & overdamped \\ = 0 & criticallydamped \\ < 0 & underdamped \end{cases} \tag{5}$$

$$p = \frac{R}{2L} \tag{6}$$

$$\omega_0 = \frac{1}{\sqrt{LC}} \tag{7}$$

$$\omega_1 = \sqrt{\omega_0^2 - p^2} \tag{8}$$

The underdamped case is typical of pulse forming networks for FRC formation. This solution has a characteristic damping coefficient, undamped resonant frequency, and natural frequency given by Eqns. 6, 7, and 8, respectively. A typical waveform is shown in Figure 5. The current oscillates in the system and decays over time due to the circuit resistance. From this waveform some important parameters for pulse discharge network design can be determined. Peak current is the maximum current achieved by the waveform and is usually the first peak in the waveform. Rise time is defined as the time from the start of the pulse to the peak current. The pseudoperiod is defined as the time between oscillations. Examples of these parameters are shown in Figure 5.

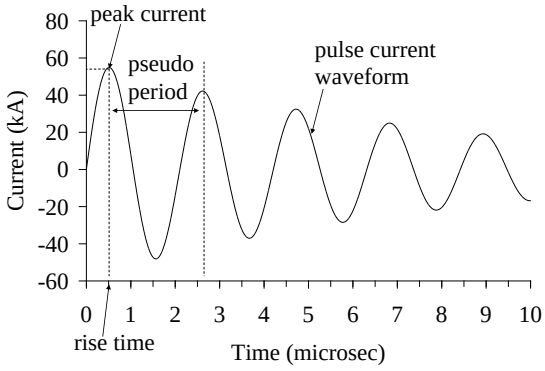

Figure 5. Example underdamped LRC circuit current waveform

B. Resistance & Inductance Determination

In a typical discharge network, resistance, inductance, and capacitance exist due to the presence of the transmission line, coil, and capacitor bank. However, simply using the DC circuit resistance and coil inductance in the LRC model can yield erroneous results. Other factors, such as the presence of the plasma, skin depth effects, and transmission line capacitance and inductance also contribute. Ideally, a combined plasma-circuit model is used to study the interaction between the pulse coil and the plasma in order to ascertain the other contributions. However, estimates of the contribution of these other effects on resistance and inductance can also be determined through analysis of existing FRC devices.

Estimates of the actual resistance and inductance of an FRC pulse discharge network are determined using the discharge waveform of two propulsion FRC devices, XOCOT and PTX. Specifically, the 250 μs discharge, 500 V waveform in Ref. 21and the 35 kV waveform in Ref. 23 are used for the analysis. These experiments are chosen because the device size and network characteristics are within the desired design parameter space. A waveform is fitted to these data, allowing the damping and frequency to be calculated. Using the determined damping coefficient, undamped resonant frequency, and the known capacitance bank sizes, the resistance and inductance are determined for each system from Eqn. 9 and 10, respectively. Finally, each coil resistance and inductance can be calculated using Eqn. 11 and 12. Subtracting out the previously calculated total system, only the other contribution are left.

$$R = \frac{2p}{C\ \omega_1^2 + p^2} \tag{9}$$

$$L = \frac{1}{\omega_0^2 C} \tag{10}$$

$$R_{coil} = \frac{\rho W}{A} \tag{11}$$

$$L_{coil} = \frac{A\mu_o}{W} \tag{12}$$

As Table 1 shows, the contribution of the effects in each device is similar and dominates the network resistance and inductance. The data show that there is only a 33 mΩ and 1.7μH difference between the two devices. The PTX values are selected for the baseline discharge network model because PTX is most closely related to the envisioned test article.

C. Design Parameter Space

The parameters varied for this study are capacitance, voltage, coil diameter, inductance, and resistance. Table 2 lists the parameters and range limits that are utilized for determining the pulse discharge network. The capacitance and voltage are relatively easily adjusted by selecting a larger or smaller capacitor bank and increasing/decreasing the bank voltage. The parameter space is designed based on circuit parameters from other FRC propulsion devices and should provide an adequate range of analysis covering anticipated circuit parameters for the FRC test article. A baseline model, see Table 3, is established so that as changes are made the corresponding effect on pulse current waveform and design acceptability is easily recognized. Hardware availability is taken into account on the capacitance design space and the coil length and diameter are established with a 3:1 ratio to minimize coil end effects and approximate an ideal solenoid.

Table 1. Calculated circuit parameters for PTX and XOCOT.

	Inductance (μH)		Resistance (mΩ)	
	PTX	**XOCOT**	**PTX**	**XOCOT**
Total	0.16	1.8	50	17
Coil	0.04	0.04	3.7×10^{-3}	2.9×10^{-4}
Other	0.12	1.8	50	17

Table 2. Varied parameter ranges

	Range	
Parameters Varied	**Lower**	**Upper**
Capacitance (μF)	0.01	10
Voltage (kV)	10	40
Inductance (μH)	0.01	10
Resistance (mΩ)	1	100
Coil Diameter (cm)	10	20

IV. Design Criteria

The goal of the pulse forming network parametric study is to determine the circuit parameters required to generate a fast current pulse that is capable of auto-ionizing a low pressure gas and providing a current reversal faster than the magnetic diffusion time of the plasma. Further, sufficient magnetic field for confinement and compression of the plasma is also desired. Achieving these goals with low voltage and low capacitance is desirable to minimize physical size of the setup. Physical size generally increases with both voltage and capacitance. The following sections describe the design criteria used to determine the optimum circuit parameters.

Table 3. Baseline model parameters.

Parameter	Value
Capacitance (μF)	1.0
Voltage (kV)	20.5
Coil Length (cm)	24.0
Coil Thickness (cm)	1.0
Coil Diameter (cm)	8.0
Resistance (mΩ)	50
Inductance (μH)	0.13

A. Auto-ionization

Auto-ionization with the current pulse is desirable to eliminate the need for a high-voltage pre-ionization source. A time-varying current through the pulse coil generates a time-varying magnetic field. From Faraday's law, a time-varying magnetic field creates an electric field. In the proposed cylindrical setup as shown in Figure 6, the azimuthal current around the coil creates an axial time-varying magnetic field, which in turn creates an azimuthal electric field that is opposite in direction to the current. If the current pulse is fast enough, the azimuthal electric field will be strong and sufficient to breakdown a low pressure gas. This type of auto-ionization from a fast current pulse has been used in other FRC devices.[23]

$$B = \frac{\mu_o i}{W} \tag{13}$$

$$E_\theta = -\frac{r}{2}\frac{dB_z}{dt} \tag{14}$$

A simple model can be used to determine the peak current and rise time required to generate an electric field sufficient to breakdown a low pressure gas. The magnetic field inside the coil of Figure 6 can be approximated as an ideal solenoid if the width-to-diameter ratio is large. In this case, the internal magnetic field is uniform and given by Eqn. 13.[28] Assuming a purely axial magnetic field and azimuthal electric field, Faraday's law reduces to Eqn. 14. For a given set of circuit parameters, Eqn. 4 is solved for the current waveform. Eqn. 13 can then be used to determine the magnetic field as a function of time and then Eqn. 14 can be used to determine the electric field. Comparison of the electric field with the known breakdown field strength for gases of interest at a given pressure (namely argon and xenon) is used to determine if the circuit parameters lead to auto-ionization of the gas.

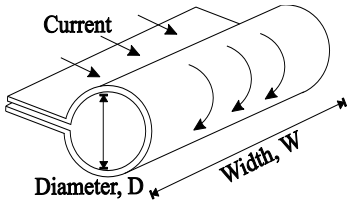

Figure 6. Example geometry for the theta pinch coil.

Breakdown voltage of a gas at a given pressure was first studied by Paschen and resulted in well-known Paschen curves. Paschen curves for argon, xenon, and hydrogen are shown in Figure 7.[29,30] Based on these data, xenon will be the most difficult to ionize, so xenon is used as the design criteria gas. In other words, if the pulse forming network can generate an electric field sufficient to ionize xenon, it is also sufficient to ionize argon and hydrogen. A pressure on the order of 10 mTorr is typical for this type of device, which, based on the Paschen curve data, yields required electric field strength on the order of 1600 V/m. We include a factor of 5 safety and require that the electric field be 8,000 V/m.

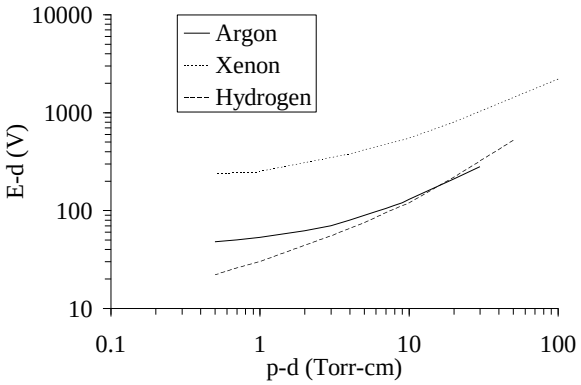

Figure 7. Paschen breakdown curves for gases of interest.

B. Magnetic Diffusion Time

Plasma is a diamagnetic conductive fluid that can be manipulated with magnetic and electric fields. As a magnetic or electric field is applied, free plasma charges redistribute themselves in an attempt to cancel out the applied field. However, this redistribution process is not instantaneous and the speed at which it occurs is related to the resistivity (or conductivity) of the plasma. For instance, in a highly conductive fluid, electrical charge can quickly relocate and easily cancel the applied field. In this case, a long time (infinite time for a perfect conductor) is required for the field to permeate the plasma fluid. In the case of magnetic fields, a magnetic diffusion time is defined to be the characteristic time required for the magnetic field to permeate the plasma.

In a successful FRC device, the current pulse waveform has a reversal time faster (smaller) than the magnetic diffusion time. This ensures that magnetic flux already present in the plasma remains trapped because it does not have sufficient time to diffuse out of the plasma. The time required for current reversal can be obtained from the current waveform and is related to the pseudoperiod (see Figure 5). Specifically, the current reversal time is the time from peak current to minimum current and is equivalent to half the pseudoperiod. An approximate magnetic diffusion time can be obtained from plasma theory and is described next.

$$\tau = \frac{\mu_o L^2}{\eta} \tag{15}$$

$$\eta \approx 5.2x10^{-5} \frac{Z \ln \Lambda}{T_e^{3/2}} \tag{16}$$

The magnetic diffusion time is related to the resistivity of the plasma and is given in Eqn. 15, where η is the plasma resistivity and L is a characteristic length. For the proposed device, the characteristic length for magnetic diffusion into and out of the plasma is the radius of the coil and we assume that the resistivity of the plasma can be approximated using the Spitzer resistivity for hydrogen, Eqn. 16.[31] These relationships are plotted in Figure 8 for a coil diameter of 0.15 m.

Previous experiments with heavy gas FRCs have shown that plasma temperature is typically on the order of 20 eV or less. From Figure 8, between 2 and 20 eV, the magnetic diffusion time varies from 40 to 1250 μs. Based on these results, we have set the design requirement at a maximum current reversal time of 10 μs. This is 2 orders of magnitude faster than the diffusion time at 20 eV and should ensure that the current and magnetic field reverse faster than magnetic flux diffuses out of the plasma.

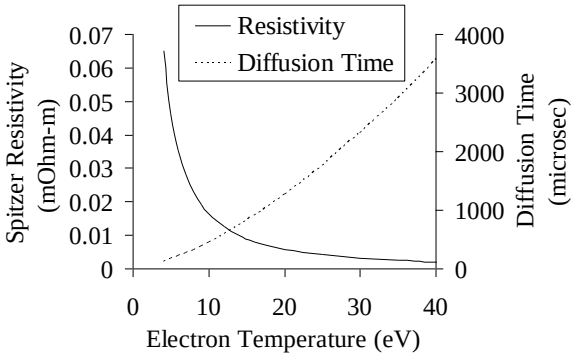

Figure 8. Spitzer plasma resistivity and magnetic diffusion time vs. plasma electron temperature.

C. Peak Magnetic Field Strength

The magnetic field in an FRC formation device is important for confining, compressing, and heating the

plasma. In general, large magnetic fields are required (~100 – 1000's of Gauss). Because the current oscillates in the system, so does the magnetic field. Based on information from previous FRC devices, we have chosen a peak magnetic field strength greater than 1000 G. All investigated circuit parameter sets are subject to the criteria that the peak magnetic field calculated with Eqn. 13 must be greater than or equal to 1000 G.

V. Design Parameter Study Results

In the following sections, the results of the parametric study are presented to establish the size of several components in this pulse discharge network. Initial results regarding the effects of resistance, inductance, capacitance, and charging voltage on a circuit are ascertained through the use of the base network model. These effects along with the specified design are used to determine the optimum circuit parameters. All possible combinations of circuit parameters are simulated to determine the values that provide the widest range of possible resistance and inductance.

A. Resistance & Inductance Effects

Analysis is conducted to ascertain the effect of resistance and inductance on the pulse current waveform. The network configuration for this analysis is the base model as described in an earlier section. Resistance is varied from 10 mμ to 60 mμ and inductance is varied from 0.05 μH to 2.15 μH. Results show that resistance only effects peak current and thus peak magnetic field. It does not effect the current reversal time. Peak current decreases 5 kA and peak magnetic field strength decreases 360 G as network resistance increases from 10 to 60 mμ. Current reversal time is a constant value of 1.1 μs for all resistance values. As inductance increases, peak current and peak magnetic field strength decrease. Data indicate a 54 kA peak current decrease, resulting in a 2850 G decrease in magnetic field strength. Current reversal time increases by 4.0 μs as the inductance increases. While the decreases in peak current and magnetic field strength seem significant, these variations can be overcome by sizing the capacitor and voltage to compensate for the difference.

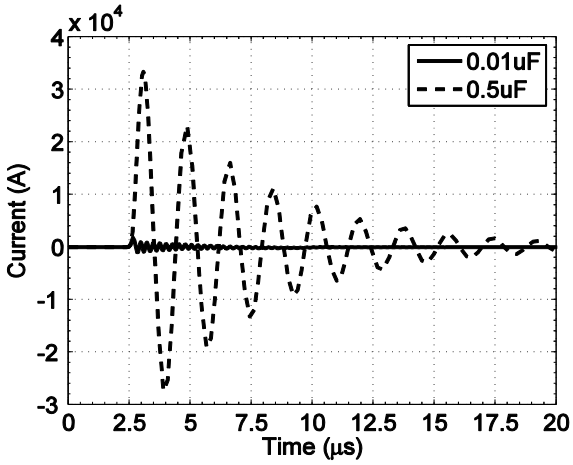

Figure 9. Current waveforms for 0.01 μF and 0.5 μF capacitance.

B. Capacitance & Voltage Effects

Capacitance is varied from 0.01 μF to 40 μF for 20.5 kV to determine the effect on the discharge network. Figure 9 illustrates the effect capacitance variation has on the current waveform. The figure shows the waveform for 0.01 μF and 0.5 μF capacitance. Increased capacitance results in an increase in both peak current (and thus increase in magnetic field strength) and current reversal time. These results are expected based on simple

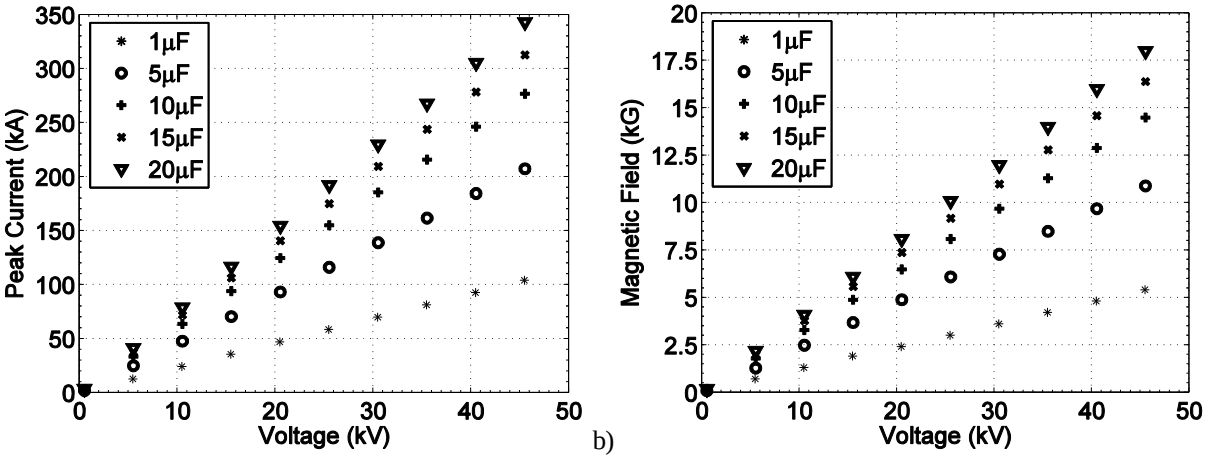

a) b)

Figure 10. a) Peak current and b) peak magnetic field strength as a function of charging voltage for multiple values of circuit capacitance.

circuit theory. For the same charging voltage, an increase in capacitance results in more charge on the capacitor so the amount of charge transferred in a given time (i.e., current) increases. Also, an increase in capacitance causes a decrease in frequency according to Eqn. 7, so current reversal time increases. Figure 10 and Figure 11 further illustrate these trends.

Figure 10 shows peak current and peak magnetic field strength as a function of capacitance and charging voltage for the baseline model (Table 3). As voltage and capacitance increase, peak current and subsequently peak magnetic field strength increase. Again, this is due to the fact that increasing voltage and/or increasing capacitance provides more initial charge on the capacitor. The increase in charge provides an increase in current and magnetic field strength. At a charging voltage of 25 kV with 1 μF of capacitance, the peak current and magnetic field strength are 55 kA and 2.6 kG, respectively. Initial analysis of peak current and magnetic field strength over the entire capacitance range (Table 2) indicates that, for a 20.5 kV charging voltage, capacitance values greater than 0.25 μF are required. This is due to the fact that lower capacitance provides lower peak current and subsequently reduced magnetic field such that it does not meet the design criteria of 1000 G.

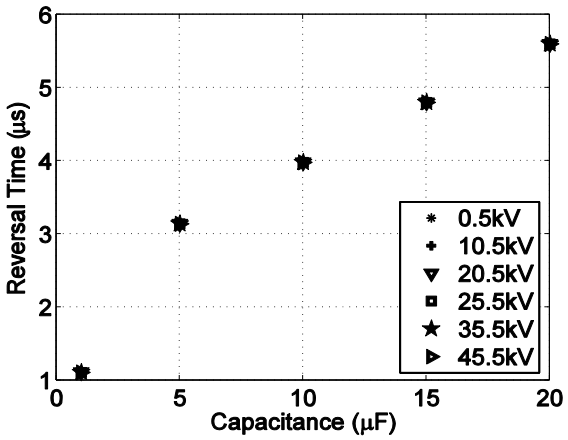

Figure 11. Reversal time as a function of capacitance for multiple charging voltages.

Figure 11 shows the current reversal time as a function of capacitance for multiple charging voltages for the baseline model. Reversal time is related to the natural frequency of the circuit and is a function of capacitance (as illustrated in Eqn. 7), but is not dependent on charging voltage. Figure 11 shows that as capacitance increases, reversal time increases. This is expected based on Eqn. 7. As capacitance increases, natural frequency decreases resulting in a longer period and larger reversal time. At a charging voltage of 25 kV with 1 μF of capacitance, the reversal time is approximately 1.2 μs. For a capacitance less than 1 μF, the reversal time is less than 1 μs, corresponding to a natural frequency greater than approximately 500 kHz. Faster reversal time and higher frequency becomes increasingly challenging for data acquisition. So, capacitance greater than or equal to 1 μF is desirable. Near the upper bound of capacitance, reversal time approaches the maximum 10 μs design limit. As a result, the capacitance upper bound is set less than 20 μF. At this maximum capacitance, the current reversal time is still less than the maximum 10 μs limit even if inductance increases to 2.15 μH.

A method for developing the optimum circuit parameters can be devised based on these results. First, capacitance is adjusted to set current reversal time. Then voltage is varied to obtain the desired peak current, peak magnetic field strength, and electric field strength.

C. Optimum Circuit Parameters

A simple Matlab code is used to simulate the waveform for each possible combination of the parameters listed in Table 2 and used to determine the optimum circuit parameters. Over 413,000 combinations are investigated, of which 80,500 provide results that meet or exceed the design criteria requirements. Specifically, the requirements are an azimuthal electric field greater than 8 kV/m, current reversal time less than 10 μs, and magnetic field strength greater than 1000 G. The following analysis first examines the voltage and capacitance combinations that provide the widest range in resistance and inductance over which the design criteria are satisfied. Then the maximum and minimum inductance provided by each voltage and capacitance combination is considered. Finally the optimum circuit parameters are selected for future construction of the FRC formation test article.

The three main design criteria are insufficient to enable selection of a single set of parameters. So, further assessment is required to reduce the available combinations. In general, capacitance and voltage are user-selected variables that can be adjusted by choosing a larger capacitor or increasing/decreasing voltage. However, the inductance and resistance of the pulse forming circuit are more difficult to adjust and control because plasma and transmission line effects can become substantial and dominate the circuit, as shown in section III-B. Therefore it is advantageous to choose a capacitor and voltage combination that provides a wide range of inductance and resistance values over which the circuit still meets the design criteria. Calculation of the number of such combinations for a given capacitance and voltage combination is given in Figure 12a. The y-axis shows the number of solutions that meet or exceed the design criteria, while the x-axis represents the combinations of voltage and capacitance. Since

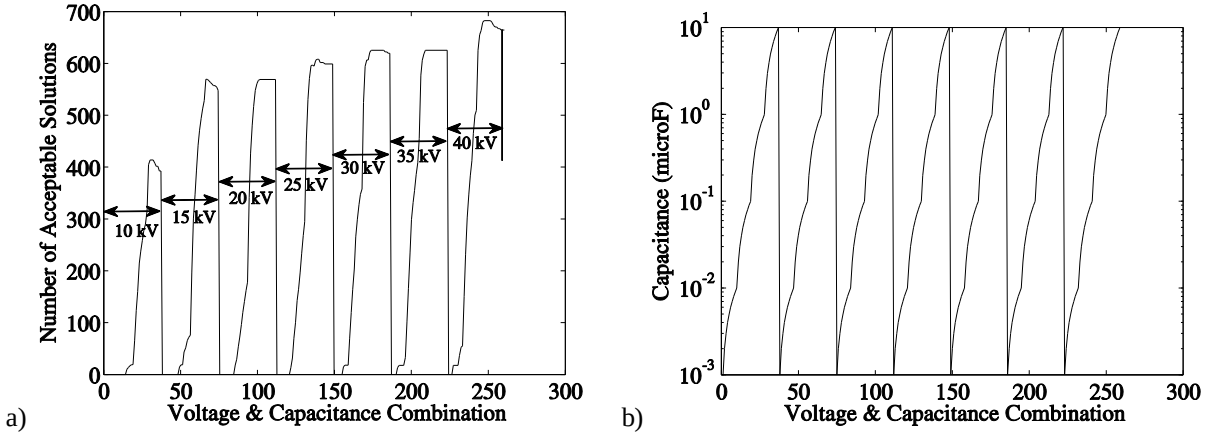

a) b)

Figure 12. Circuit simulation results for all possible combinations of voltage and capacitance. a) Total simulation solutions that meet the design criteria and b) capacitance for each combination investigated.

there are 7 voltage values and 37 capacitance values investigated, there are a total of 259 voltage-capacitance combinations. For instance, an x-axis value between 0 and 37 corresponds to a voltage of 10 kV, and each of the 37 points within this range corresponds with a different capacitance value, as shown in Figure 12b.

Results show that to achieve a maximum range in inductance and resistor values over which the desired criteria are satisfied, high-voltage and relatively high capacitance is required. From Figure 12a, as voltage increases, the number of acceptable solutions increases, i.e., a wider choice in inductance and resistance. Also, for a given voltage, Figure 12a shows that a capacitance within the range of a few 100 nF to a few μF is best.

Two competing processes dictate the trends with capacitance. For each voltage, low capacitance provides almost zero acceptable solutions. This is due to the fact that low capacitance provides small peak current that is insufficient to generate the required magnetic field. However, when capacitance is high, the number of acceptable solutions also decreases. This is due to the fact that increasing capacitance increases the current reversal time to the point where it is larger than the design requirement.

Circuit inductance is very important for obtaining the desired criteria. Based on previous calculations, the PTX experiment has an inductance on the order of a 0.16 μH. The PTX criteria is used because the proposed FRC test article is most similar to the PTX experiment. Operation of the test article at or above this inductance value may be necessary to achieve the desired performance. Figure 13 shows the maximum and minimum inductance values that provide acceptable solutions for the investigated combinations of voltage and capacitance. Simulation results show that only voltages greater than or equal to 25 kV provides acceptable solutions with an inductance above 0.16 μH. This result provides the minimum acceptable voltage for the test article, 25 kV.

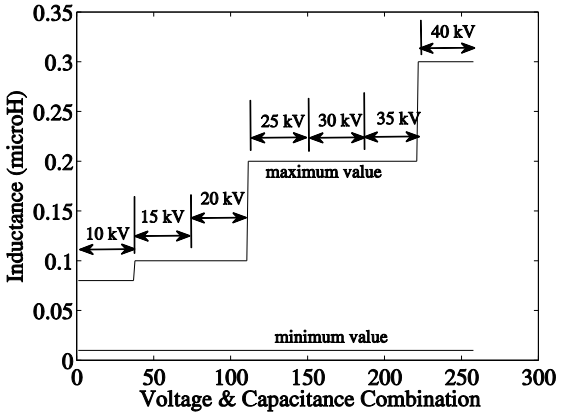

Figure 13. Maximum and minimum inductance for the investigated voltage and capacitance combinations.

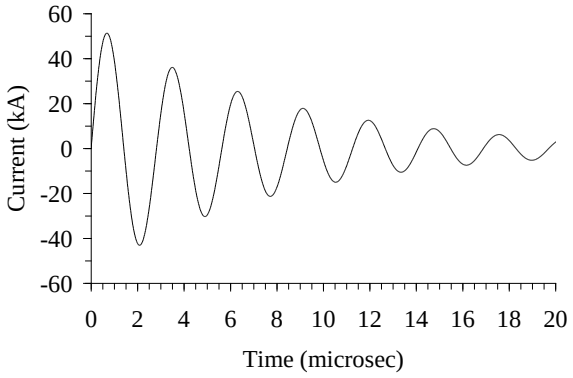

Figure 14. Current waveform for the optimum circuit capacitance and voltage, assumed resistance and inductance of 50 mΩ and 0.2 μH, respectively

The circuit parameter analysis indicates that a voltage of 25 kV and capacitance of 1 μF are optimum. The minimum acceptable voltage of 25 kV is chosen to reduce issues associated with higher voltage, such as switching, shielding, stand-off distance, insulation, etc. A capacitance of 1 μF is chosen because it provides the widest range in resistance and inductance that still satisfies the design criteria. The expected waveform for these parameters, assuming a circuit resistance and inductance of 50 mΩ and 0.2 μH is shown in Figure 14. It provides a peak current of 51 kA, peak magnetic field of 2 kG for a 0.45 m coil width, a rise time of 0.7 μs, and current reversal time of 1.4 μs.

VI. Conclusion & Future Work

From the parametric analysis general trends and an optimum pulse discharge network are obtained. In the analysis, the effects of component sizing on the pulse discharge network have been established through the use of the baseline model. Results show that capacitance sets pseudoperiod, rise time, and reversal time, while voltage sets peak current and magnetic field strength. Based on the established design criteria (electric field strength of 8 kV/m, reversal time less than 10 μs, and magnetic field strength greater than or equal to 1000 G) several combinations of network parameters are possible; however, the optimum design provides the widest range of possible resistance and inductance. This allows for variation in actual resistance and inductance from the preliminary values while maintaining desirable network output. The optimum parameters of the discharge network established in this study are as follows: 1 μF capacitance, 25 kV charging voltage, resistance of 50 mμμ and 0.2 μH inductance.

Given the information obtained from this parametric study, further progress can be made using MHD simulations and test articles. A parametric study on the discharge coil geometry will need to be completed to ascertain desired discharge coil results. MHD simulations will be used to confirm the results of the preliminary analysis presented and to establish the plasma contributions for a given pulse forming network. Development of a test article will begin to verify results of preliminary analysis and simulations. Components can be selected based on the preliminary information since the network covers a wide range of resistance and inductance.

Acknowledgments

The authors would like to thank the NASA-Missouri Space Grant Consortium and University of Missouri Research Board for providing support for this work. We would also like to thank the research team of the Aerospace Plasma Laboratory for helpful suggestions over the course of this work.

References

[1]Gulczinski III, F. S., Spores, R. A., "Analysis of Hall-effect thrusters and ion engines for orbit transfer missions," AIAA-96-2973, *32nd Joint Propulsion Conference*, Lake Buena Vista, FL, July 1-3, 1996.

[2]Spores, R. A., Spanjers, G. G., Birkan, M., Lawrence, T. J., "Overview of the USAF Electric Propulsion Program," AIAA-2001-3225, *37th Joint Propulsion Conference*, Salt Lake City, UT, July 8-11, 2001.

[3]Spores, R. A., Birkan, M., "Overview of USAF Electric Propulsion Program," AIAA-2002-3558, *38th Joint Propulsion Conference*, Indianapolis, IN, July 7-10, 2002.

[4]Sutton, G. P., Biblarz, O., *Rocket Propulsion Elements*, 7th Ed., John Wiley & Sons, Inc., New York, 2001.

[5]Jahn, R. G., *Physics of Electric Propulsion*, McGraw-Hill Book Company, New York, 1968.

[6]Manzella, D. H., Jankovsky, R., Hofer, R. R., "Laboratory Model 50 kW Hall thruster," AIAA-2002-3676, *38th Joint Propulsion Conference*, Indianapolis, IN., July 7-10, 2002.

[7]Hargus, W. A., Reed, G., "The Air Force Clustered Hall Thruster Program," AIAA-2002-3678, *38th Joint Propulsion Conference*, Indianapolis, IN., July 7-10, 2002.

[8]Randolph, T., Dougherty, R. C., Oleson, S., Fiehler, D., Dipprey, N., "The Prometheus 1 Spacecraft Preliminary Electric Propulsion System Design," AIAA-2005-3889, *41st Joint Propulsion Conference*, Tucson, AZ, July 10-13, 2005.

[9]Bellan, P. M., *Spheromaks: A Practical Application of Magnetohydrodynamic Dynamos and Plasma Self-Organization*, Imperial College Press, London, 2000.

[10]Goldenbaum, G. C., Irby, J. H., Chong, Y. P., Hart, G. W., "Formation of a Spheromak Plasma Configuration," *Physical Review Letters*, Vol. 44, No. 6, pp. 393-396, Feb. 1980.

[11]Tuszewski, M., Armstrong, W. T., Chrien, R. E., Klingner, P. L., McKenna, K. F., Rej, D. J., Sherwood, E. G., Siemon, R. E., "Confinement of translated field-reversed configurations," *Physics of Fluids*, Vol. 29, No. 3, pp. 863-870, March 1986.

[12]Rej, D. J., Armstrong, W. T., Chrien, R. E., Klinger, P. L., Linford, R. K., McKenna, K. F., Sherwood, E. G., Siemon, R. E., Tuszewski, M., Milroy, R. D., "Experimental studies of field-reversed configuration translation," *Physics of Fluids*, Vol. 29, No. 3, pp. 852-862, March 1986.

[13]Taccetti, J. M., Intrator, T. P., Wurden, G. A., Zhang, S. Y., Aragonez, R., Assmus, P. N., Bass, C. M., Carey, C., deVries, S. A., Fienup, W. J., Furno, I., Hsu, S. C., Kozar, M. P., Langner, M. C., Liang, J., Maqueda, R. J., Martinez, R. A., Sanchez, P. G., Schoenberg, K. F., Scott, K. J., Siemon, R. E., Tejero, E. M., Trask, E. H., Tuszewski, M., Waganaar, W. J., Grabowski, C.,

Ruden, E. L., Degnan, J. H., Cavazos, T., Gale, D. G., Sommars, W., "FRX-L: A field-reversed configuration plasma injector for magnetized target fusion," *Review of Scientific Instruments*, Vol. 74, No. 10, pp. 4314-4323, Oct. 2003.

[14]Tuszewski, M., "Excluded flux analysis of a field-reversed plasma," *Physics of Fluids*, Vol. 24, No. 11, pp. 2126-2127, Nov. 1981.

[15]Rej, D. J., Tuszewski, M., "A zero-dimensional transport model for field-reversed configurations," *Physics of Fluids*, Vol. 27, No. 6, pp. 1514-1520, June 1984.

[16]Jurczyk, B. E., Stubbers, R. A., "Edge Localized Mode Simulating Plasma Gun," DOE SBIR Phase I Final Report, DE-FG02-04ER86339, 2004.

[17]Slough, J., Votroubek, G., "Magnetically Accelerated Plasmoid (MAP) Propulsion," AIAA-2006-4654, *42nd Joint Propulsion Conference*, Sacramento, CA, July 9-12, 2006.

[18]Slough, J. T., "Propagating Magnetic Wave Plasma Accelerator (PMWAC) for Deep Space Exploration," NASA Institute for Advanced Concepts Phase I Final Report, 359, MSNW, Bellevue, WA, 1999.

[19]Slough, J. T., "Earth to Orbit based on a Reciprocating Plasma Liner Compression of Fusion Plasmoids," AIAA-2007-5130, *43rd Joint Propulsion Conference*, Cincinnati, OH., July 8-11, 2007.

[20]Kirtley, D., Brown, D. L., Gallimore, A. D., "Details on an Annular Field Reversed Configuration Plasma Device for Spacecraft Propulsion," IEPC-2005-171, *29th International Electric Propulsion Conference*, Princeton, NJ., Oct. 31- Nov. 4, 2005.

[21]Kirtley, D. E., "Study of the Synchronous Operation of an Annular Field Reversed Configuration Plasma Device," Doctoral Thesis, Dept. of Aerospace Engineering, The University of Michigan, Ann Arbor, MI, 2008.

[22]Kirtley, D., Gallimore, A. D., Haas, J., Reilly, M., "High Density Magnetized Toroid Formation and Translation within XOCOT: An Annular Field Reversed Configuration Plasma Concept," IEPC-2007-041, *30th International Electric Propulsion Conference*, Florence, Italy, Sept. 17-20, 2007.

[23]Koelfgen, S. J., Eskridge, R., Lee, M. H., Martin, A., Hawk, C. W., Fimognari, P., "Magnetic and Langmuir Probe Measurements on the Plasmoid Thruster Experiment (PTX)," AIAA-2004-4094, *40th Joint Propulsion Conference*, Fort Lauderdale, FL., July 11-14, 2004.

[24]Koelfgen, S. J., Hawk, C. W., Eskridge, R., Lee, M. H., Martin, A., Smith, J. W., "A Plasmoid Thruster For Space Propulsion," AIAA-2003-4992, *39th Joint Propulsion Conference*, Huntsville, AL, July 20-23, 2003.

[25]Slough, J. T., Kirtley, D., Weber, T., "Pulsed Plasmoid Propulsion: The ELF Thruster," IEPC-2009-265, *31st International Electric Propulsion Conference*, Ann Arbor, MI, Sept. 20-24, 2009.

[26]Fimognari, P. J., Cassibry, J. T., Ims, K.-E., "Effects of Pre-ionization and Bias Field on Plasmoid Formation and Acceleration," AIAA-2007-5262, *43rd Joint Propulsion Conference*, Cincinnati, OH, July 8-11, 2007.

[27]Niemela, C. S., King, L. B., "Numerical Optimization of an Annular Field Reversed Configuration Translation Experiment," IEPC-2009-008, *31st International Electric Propulsion Conference*, Ann Arbor, MI, Sept. 20-24, 2009.

[28]Halliday, D., Resnick, R., Walker, J., *Fundamentals of Physics*, Fifth Ed., John Wiley & Sons, Inc., New York, 1997.

[29]Brown, S. C., *Basic Data of Plasma Physics*, The M.I.T. Press, Cambridge, MA, 1959.

[30]Kruithof, A. A., "Townsend's Ionization Coefficients for Neon, Argon, Krypton, and Xenon," *Physica*, Vol. 7, pp. 519, 1940.

[31]Chen, F. F., *Introduction to Plasma Physics and Controlled Fusion*, Vol. 1: Plasma Physics, Plenum Press, New York, 1984.